Journal of Membrane Science 361 (2010) 191–205

Contents lists available at ScienceDirect

Journal of Membrane Science

journal homepage: www.elsevier.com/locate/memsci

Fouling behavior of electroacidified soy protein extracts during cross-flow ultrafiltration using dynamic reversible–irreversible fouling resistances and CFD modeling

Amin Reza Rajabzadeh [a], Christine Moresoli [a,*], Bernard Marcos [b]

[a] Chemical Engineering Department, University of Waterloo, 200 University Avenue West, Waterloo, Ontario, N2L 3G1 Canada
[b] Département de génie chimique et génie biotechnologique, Université de Sherbrooke, Sherbrooke, J1K 2R1 Canada

ARTICLE INFO

Article history:
Received 13 November 2009
Received in revised form 25 May 2010
Accepted 28 May 2010
Available online 4 June 2010

Keywords:
Computational fluid dynamics (CFD)
Ultrafiltration
Soy protein
Electroacidification
Fouling

ABSTRACT

The transient membrane fouling during the concentration by cross-flow ultrafiltration of soy protein extracts subjected to electroacidification is examined by combining experimentation with computational fluid dynamics (CFD) modeling. Transient reversible (water removal) and irreversible (chemical removal) membrane fouling resistances, permeate flux, protein concentration and protein concentration dependent viscosity were obtained experimentally. A detailed fouling resistance model to describe the reversible and the irreversible fouling resistances was developed in terms of the microscopic local transient and spatial pressure difference, permeate velocity, protein concentration and initial fouling resistance conditions. This fouling resistance model is used in a boundary condition for the permeate velocity when solving the momentum and protein concentration continuity equations with CFD. The model estimates agree with experimentally measured permeate flux, protein concentration and transient irreversible and reversible fouling resistances. In particular, the model estimated accurately the transient reversible and irreversible fouling resistances, a limitation of most previously published models. The model shows considerable axial variation of the reversible fouling resistance and the protein concentration at the membrane surface which supports the inadequacy of the film theory and the assumptions for constant properties. In contrast, the irreversible fouling resistance remains relatively constant with axial position suggesting protein adsorption.

1. Introduction

Membrane ultrafiltration (UF) is a pressure driven operation where liquid and solutes smaller than the membrane pores permeate through a membrane while solutes larger than the membrane pores are retained. The accumulation of solutes near the membrane surface or within the membrane pores constitutes membrane fouling. Major efforts have been devoted to study fouling and design more efficient ultrafiltration membrane systems. However, the complexity of fouling has limited the progress to better understand and predict the occurrence of fouling. Modeling studies represent an attractive alternative to obtain information on the contribution of the feed properties and the operating conditions to membrane fouling. In particular, mathematical microscopic methods constitute an attractive approach for the investigation of fouling mechanisms near the membrane surface. These methods are based on numerically solving Navier–Stokes equations and the continuity equation with additional relationships describing fouling. Analytical solutions are nearly impossible to obtain due to the complexity of these equations. Some approximated solutions can be used to solve the Navier–Stokes equations [1,2] and can be combined with a complete numerical solution of the continuity equation. In some cases, the microscopic model considers a spatial or transient fouling model in the boundary condition to determine the local permeate velocity and the convection-diffusion equation for species material balance. For instance, Yeh et al. [3] combined a simplified steady state momentum equation with a resistance-in-series model where the gel layer resistance is proportional to the local transmembrane pressure to describe dextran ultrafiltration. Tu et al. [4] used simplified partial differential equations for the continuity equation and computed the transient permeate velocity at the wall from a resistance-in-series model representing internal pore fouling, concentration polarization and gel layer mechanisms. The dynamics of the different resistances were represented by ordinary differential equations with power law relationship for the resistances in terms of concentrations and pressure. To describe a hollow-fiber UF configuration, Secchi et al. [5] used the resistance-in-series model as a boundary condition of the continuity equation. The resistance-in-

* Corresponding author. Tel.: +1 519 888 4567x35254.
E-mail address: cmoresol@uwaterloo.ca (C. Moresoli).

0376-7388/$ – see front matter © 2010 Elsevier B.V. All rights reserved.
doi:10.1016/j.memsci.2010.05.057

series model consisted of the intrinsic membrane resistance and an adsorption resistance with a Langmuir form for the solutes retained at the membrane surface.

When the approximated relations for the Navier–Stokes and continuity equations are not sufficient, in house or commercial computational fluid dynamics (CFD) codes are required. During the last decade, a number of studies have illustrated the use of CFD modeling for solving the complete set of continuity and momentum equations for membrane filtration [6–11]. The advantages of CFD modeling for the understanding of the filtration process have been presented by Ghidossi et al. [12]. CFD models can provide a rigorous and detailed analysis of the local and transient conditions for the permeate velocity, the solute concentration and the fouling with a reduced number of assumptions. For example, estimates of the transient and local permeate flux and fouling behavior were obtained without requiring assumptions on the polarization layer thickness [11]. The conditions at the membrane surface were described by a dynamic resistance-in-series model, based on the experimental permeate flux profile for the concentration of soy protein extracts by cross-flow ultrafiltration [11]. The model, validated with experimental permeate flux and protein concentration data, predicted axial variations of the protein concentration at the membrane surface with a maximum occurring before the end of the filter. The existence and importance of axial variations of the permeate velocity and solute concentration during membrane ultrafiltration of dextran solutions was also reported by Ma et al. [13] using a finite element model for solving Navier–Stokes and the continuity equations. The permeate velocity at the membrane surface was represented by the osmotic pressure model expressed in terms of dextran concentration. The concentration dependency of the viscosity was also shown to be a critical factor for the prediction of a limiting flux, the pressure independent flux, for the concentration of dextran solutions. The approach proposed by Ma et al. [13] assumes the existence of limiting flux and steady-state conditions. Schausberger et al. [14] developed a transient finite volume code and solved the mass, momentum and species conservation equations for the cross-flow ultrafiltration of BSA with total BSA retention. The model incorporated detailed osmotic pressure, viscosity and diffusion coefficient representation for BSA. The fouling was described with a modified Darcy's law and a resistance-in-series model with an irreversible surface adsorption fouling reaction. A one adjustable parameter model was developed. Excellent agreement with the model and experimental data was obtained for the permeate flux and different pH and feed velocity conditions. The agreement was not so good for the effect of protein concentration and the concentration polarization and fouling which could be due to membrane–solute interactions that are neglected in this model.

Soy protein ingredients are contained in a wide variety of processed food products. A number of studies describe the advantages of membrane UF for the production of soy protein ingredients with improved protein yields and functional properties [15–17]. The membrane pore size is generally selected to enable the removal of carbohydrates and minerals by permeation through the membrane while retaining and concentrating the major soy proteins. Recent work has shown that the combination of electroacidification and UF represents an attractive approach for the concentration of soy protein extracts [17–20]. The electroacidification of the soy protein extract to pH 6 enhances the magnesium, calcium, and phytic acid removal compared with the non-electroacidified soy protein extract at pH 9. However, electroacidification decreases the permeate flux during UF which results in longer filtration time. The ionic strength and the pH are known to affect the strength and the nature of protein–protein and membrane–protein interactions. Lower electrostatic repulsion forces between the proteins at conditions near their isoelectric point results in a tighter protein accumulation on the membrane surface suggested to be responsible for the lower permeate flux observed in the UF of the electroacidified soy protein extract [17–20].

The modeling of soy protein UF has generally combined simple macroscopic models and empirical observations to describe fouling and process observations. This approach is unable to provide information on the local behavior of the filtration. Krishna Kumar et al. [16] modeled the permeate flux with the film theory mass transfer model and a resistance-in-series model to compare the performance of tubular and spiral modules for soy protein concentrates in a total recycle mode at steady-state. The total fouling resistance was represented by the sum of a concentration polarization resistance (proportional to the pressure) and a solute membrane interactions resistance. Constant and global resistances were estimated from steady-state filtration data. Furukawa et al. [21] modeled the UF of soy sauce lees considering fouling caused by the cake formation and limited by the hydraulic lift velocity. They rearranged this resistance-in-series model to introduce reversible and irreversible resistances. The reversible resistance is defined to be proportional to permeate volume. The irreversible resistance is assumed to change from a pure water membrane resistance to the total irreversible resistance observed at the initial stage of the filtration. The total irreversible resistance is assumed to remain constant during the filtration. The use of the reversible and the irreversible resistance concept is attractive because these resistances can be easily estimated experimentally and provide some explanation of the fouling mechanisms.

The present work was motivated by the desire to understand the fouling observed during the concentration of electroacidified soy protein extract in a hollow fiber ultrafiltration system. The CFD methodology recently developed by Marcos et al. [11] to describe the feed tank and the hollow fiber UF system for soy protein concentration was chosen. The model considers only the proteins and does not take into account the carbohydrates and the minerals contained in the soy protein extract. It is assumed that all the low molecular weight components, carbohydrates and minerals, permeate freely through the membrane pores such that the proteins are the only membrane foulant. This assumption is based on the experimental observations reported by Skorepova [18] where the proteins represented at least 93% of the total solids deposited on the membrane during the ultrafiltration of non-electroacidified and electroacidified soy protein extracts. The transient fouling resistances constitute a boundary condition (Darcy's law and resistance-in-series model) when solving the momentum and protein concentration continuity equations. The formulation of the dynamic resistance-in-series model in the current study differs from [11]. In the current study, we have selected a formulation that allows easily accessible experimental estimation of the fouling resistances. The global fouling resistance consists of the membrane resistance, the reversible fouling resistance (water removal) and the irreversible fouling resistance (chemical removal). A new transient fouling resistance model based on the initial fouling resistance conditions, the local permeate flux, pressure difference and protein concentration, was developed to describe the reversible and irreversible fouling resistance components. The viscosity of the soy protein extracts was considered as a function of protein concentration and pH to represent the electroacidification effect. The model was calibrated with experimental transient permeate flux and protein concentration data. Different patterns of initial and transient irreversible and reversible fouling resistances according to the pH of the soy protein solution were experimentally observed and simulated by the model. In contrast to the classical numerical modeling approach, this study takes advantage of CFD modeling tools to combine the hydrodynamics and the solute transport with the fouling behavior for a hollow fiber membrane ultrafiltration system and feed tank and obtain estimates of the spatial and transient pro-

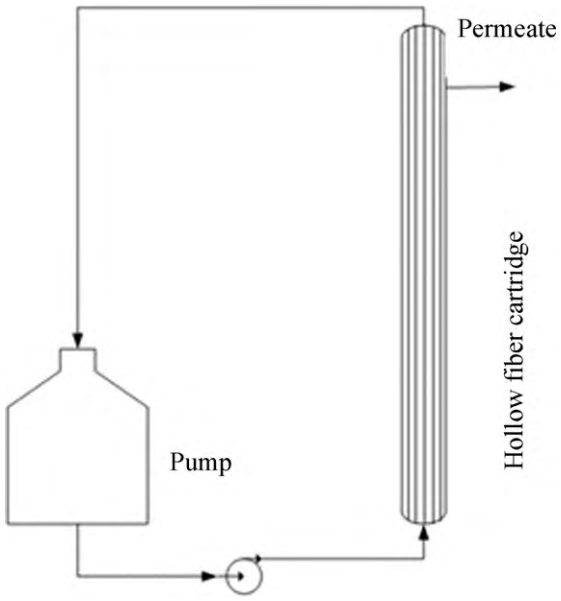

Fig. 1. Diagram of the feed tank and ultrafiltration hollow fiber module.

tein concentration and velocity profiles inside the fiber by solving the Navier–Stokes equation coupled with the continuity equation for the soy protein. The model, validated with independent experimental data, showed the effect of two operating parameters, feed velocity and transmembrane pressure, on the spatial and transient permeate velocity and protein concentration profiles. Estimates of the spatial and transient reversible and irreversible fouling resistances were also obtained and served to better understand the concentration operation and the effect of electroacidification during the ultrafiltration of soy protein extracts.

2. Modeling

2.1. Geometry and computational mesh used

The system that was modeled consisted of the feed tank and the membrane hollow fiber module (Fig. 1). During a filtration, the feed was pumped through the module and the retentate was returned to the feed tank while the permeate was collected. The hollow fiber membrane module contained 50 fibers with a 5.0×10^{-4} m radius and 0.3 m length. Every fiber was assumed identical and only one fiber was modeled. Fig. 2 presents the major hydrodynamic characteristics of a fiber.

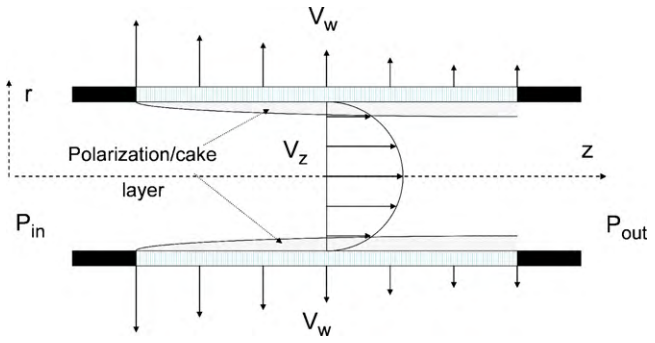

Fig. 2. Simplified representation of the hydrodynamics in the hollow fiber.

2.2. Governing equations of the hollow fiber

The governing equations, the equations for conservation of mass, protein concentration and momentum, in 2D-cylindrical coordinates are mathematically given in Eqs. (1)–(4) [11,22]. The Reynolds number is smaller than 1500 so that the flow is laminar. The equations solved are:

$$\frac{\partial v_z}{\partial z} + \frac{1}{r}\frac{\partial r v_r}{\partial r} = 0 \tag{1}$$

$$\frac{\partial C}{\partial t} + v_z\frac{\partial C}{\partial z} + v_r\frac{\partial C}{\partial r} = \frac{1}{r}\frac{\partial}{\partial r}\left(Dr\frac{\partial C}{\partial r}\right) + \frac{\partial}{\partial z}\left(D\frac{\partial C}{\partial z}\right) \tag{2}$$

$$\rho\left(\frac{\partial v_z}{\partial t} + v_z\frac{\partial v_z}{\partial z} + v_r\frac{\partial v_z}{\partial r}\right) = \frac{1}{r}\frac{\partial}{\partial r}\left(r\mu\frac{\partial v_z}{\partial r}\right) + \frac{\partial}{\partial z}\left(\mu\frac{\partial v_z}{\partial z}\right) - \frac{\partial P}{\partial z} \tag{3}$$

$$\rho\left(\frac{\partial v_r}{\partial t} + v_z\frac{\partial v_r}{\partial z} + v_r\frac{\partial v_r}{\partial r}\right) = \frac{1}{r}\frac{\partial}{\partial r}\left(r\mu\frac{\partial v_r}{\partial r}\right) + \frac{\partial}{\partial z}(\mu\frac{\partial v_r}{\partial z}) - \frac{\partial P}{\partial r} \tag{4}$$

In the previous equations, v_z and v_r are the velocity components in the z and r directions, respectively, ρ is the fluid density, P is the pressure, μ is the fluid viscosity, C is the protein concentration and D is the average protein diffusion coefficient. The density and the diffusion coefficient are assumed constant during the filtration; the viscosity varies during the filtration and depends on the protein concentration and electroacidification conditions (see Section 2.5).

2.3. Initial and boundary conditions of the fiber

At the inlet of the fiber, the flow is assumed to be fully developed and a parabolic flow is specified. The maximum velocity ($v_{z,\max}$) of the inlet parabolic flow is computed from the feed flowrate and the dimension of the fiber. The outlet pressure (P_{out}) is related to the transmembrane pressure TMP and the total pressure drop in the fiber. Furthermore, the protein concentration at the inlet of the fiber is taken to be the concentration in the feed tank

$$\text{at } z = 0, \quad v_z = v_{z,\max}\left(1 - \left(\frac{r}{R}\right)^2\right), \qquad v_r = 0, \qquad C = C_{feed}(t) \tag{5a}$$

$$\text{at } z = L, \quad P = P_{out}, \qquad \frac{\partial C}{\partial z} = 0 \tag{5b}$$

The outlet boundary condition, P_{out}, is a common boundary condition in fluid dynamics as recently used [14].

The fiber is axisymmetric therefore:

$$\text{at } r = 0, \quad \frac{\partial v_z}{\partial r} = 0, \qquad v_r = 0, \qquad \frac{\partial C}{\partial r} = 0 \tag{5c}$$

A no slip boundary condition is defined at the membrane surface [23]

$$\text{at } r = R, \quad v_z = 0, \qquad v_r = v_w \tag{5d}$$

where $v_W(z, t)$ is the permeate velocity.

It is assumed that soy proteins are totally rejected by the 100 kDa membrane (verified previously where the protein content in the permeate was approximately 2 wt% and approximately 90 wt% in the retentate for cross-flow ultrafiltration concentration operation with a similar system and operating conditions [17]). The average particle size of the electroacidified and non-electroacidified

Table 1
Physical properties of the soy protein extracts.

Model parameters	Non-electroacidified soy protein extract	Electroacidified soy protein extract
α [$m^3\,kg^{-1}$]	0.0432	0.0196
D [$m^2\,s^{-1}$]	5×10^{-11}	2.5×10^{-11}
ρ [$kg\,m^{-3}$]	997	

soy protein extracts examined in this study was estimated previously, 707 and 220 nm, respectively [19]. We also assumed that the protein adsorbed on the membrane surface (irreversible fouling) is negligible compared to the magnitude of the protein concentration at the wall.

$$\text{at } r = R, \quad v_w C - D\frac{\partial C}{\partial r} = 0 \tag{5e}$$

$$\text{at } t = 0, \quad v_z = v_{z,\max}\left(1 - \left(\frac{r}{R}\right)^2\right), \qquad v_r = 0, \qquad C = C_{feed},$$

$$P = P_{out} \tag{5f}$$

2.4. Governing equations for the feed tank

The feed tank is modeled as a well mixed continuous stirred tank. The change in the feed volume is obtained by writing a mass balance over the feed tank

$$\frac{dV_{feed}}{dt} = Q_{hf} - Q_{feed} = -Q_{Per} \tag{6}$$

No protein accumulation in the pipe between the feed tank and the hollow fiber module is assumed. With the well mixed assumption, the transient protein concentration is uniform in the feed tank. The time change in the protein concentration is therefore represented by Eq. (7) and the permeate flux is obtained by integrating the local permeate velocity at the membrane surface according to Eq. (8):

$$\frac{dC_{feed}}{dt} = \frac{Q_{Per}C_{feed}}{V_{feed}} \tag{7}$$

$$Q_{per}(t) = (2n\pi R)\int_0^L v_w(z,t)\,dz \tag{8}$$

2.5. Physical properties of the solution

The density of the soy protein solution is assumed constant during the filtration. The effect of the soy protein concentration on the viscosity of the solution, however, is considered in the model

$$\mu = \mu^0 \times (1 + \alpha C) \tag{9}$$

where μ^0 is the water viscosity at 25 °C, α is an empirical coefficient specific to the electroacidification conditions estimated experimentally by Skorepova [18], and can be found in Table 1. A constant diffusion coefficient independent of protein concentration was assumed as an initial approach. The estimated average diffusion coefficient of $5\times10^{-11}\,m^2\,s^{-1}$ was obtained from the literature for the non-electroacidified soy protein extract [24]. This value was used as a reference value to roughly estimate the diffusion coefficient for the electroacidified soy protein extract using Stokes–Einstein equation. Skorepova [18] reported that the average size of the electroacidified soy protein is 2–3 times larger than for the non-electroacidified soy protein extract. An average diffusion coefficient of $2.5\times10^{-11}\,m^2\,s^{-1}$ was used for the electroacidified soy protein extract.

2.6. Permeate flux modeling

The local permeate velocity at the membrane surface ($v_w(z,t)_{r=R}$), the boundary condition for the Navier–Stokes equation, was represented by Darcy's law (Eq. (10)) and the resistance-in-series model (Eq. (11))

$$v_w(z,t) = \frac{\Delta P(z,t)}{\mu^0 R_G} \tag{10}$$

$$R_G = R_m + R_R + R_I \tag{11}$$

$\Delta P(z,t)$ is the local transient pressure difference between the pressure $P(z,t)$ inside the membrane fiber and the pressure outside the membrane fiber at a given position z along the fiber; $\Delta P(z,t)$ varies along the membrane and during the filtration process. The pressure outside the membrane fiber is atmospheric pressure. The operating transmembrane pressure (TMP) is the average value of $\Delta P(z,t)$ estimated at the entrance and at the exit of the fiber.

In this study, we have selected a hydrodynamic approach to represent Darcy's law and the behavior of the retained components at the membrane surface. This approach includes the local transient pressure difference and sequential fouling resistances because these terms can be estimated experimentally, are directly related to the operation of the ultrafiltration process and have shown to represent accurately the concentration of soy protein extracts by ultrafiltration under similar operating transmembrane pressure and concentrations [16]. The alternative thermodynamics approach, such as the osmotic pressure approach, requires extensive experimental data according to concentration, pH and ionic strength (Schausberger [14]) or involves the analysis of complex forces interactions (Bowen [25]) to estimate accurately the multiparameter empirical osmotic pressure correlation. This was applied to BSA, a single protein solution with a five parameter osmotic pressure correlation (Schausberger [14]). We felt that this approach was not adequate for the investigation of soy proteins, a complex protein mixture. In our hydrodynamic approach, the contribution of the osmotic pressure is implicitly described by the sequential fouling resistances.

The global fouling resistance R_G, as per Eq. (11), contains the clean membrane resistance R_m, the reversible fouling resistance R_R and the irreversible fouling resistance R_I. The reversible fouling was considered surface fouling that can be removed by water. The irreversible fouling was considered to occur either on the membrane surface or inside the membrane pores and is chemically attached to the membrane. Since the soy protein extracts consist of a mixture of proteins with different molecular size, standard blocking and pore blocking could occur during the filtration. These individual mechanisms were not distinguished in this study and were grouped as irreversible fouling.

Numerous models have been presented to describe the dynamics of resistance for the resistance-in-series approach. For example, Ho and Zydney [26] proposed a combined pore blockage and cake formation model to describe protein ultrafiltration. The cake formation represents the rate of protein deposit which is assumed to be proportional to the convective transport of protein. A different approach was proposed by Kilduff et al. [27] where the rate of cake formation contains a convective transport term and a back transport term for the fouling of organic matter during nanofiltration operations. Tu et al. [4] proposed a power law approach to

Table 2
Model parameters.

	Non-electroacidified soy protein extract	Electroacidified soy protein extract
k_R [kg m^{-1}]	1.8×10^{-12}	0.8×10^{-12}
k_I [kg s m^{-3}]	1.4×10^{5}	2.0×10^{5}
$R_{I\,ss}$ [m^{-1}]	2.0×10^{12}	4.2×10^{12}
R_m [m^{-1}][a]	1.5×10^{12}	1.5×10^{12}
$R_{I\,initial}$ [m^{-1}]	5.8×10^{11}	1.31×10^{12}
β [m^{-1}]	1.5×10^{12}	0.8×10^{12}
λ [Pa^{-1}]	2.5×10^{-5}	5.7×10^{-5}
C_{feed} [kg m^{-3}]	10	10

[a] Membrane resistance was 1.5×10^{12} m^{-1} unless stated.

relate polarization, pore blocking and gel layer resistances to the major parameters and obtained the rate of formation by derivation of the power law for the fouling of organic matter during nanofiltration operations. These models were developed for a macroscopic analysis and do not consider the local variations of the wall concentration and the permeate velocity. The model proposed in this study considers the local spatial variation of the fouling resistances and their validation with experimental fouling measurements, that is to say the reversible fouling and irreversible fouling components that are related to the major fouling mechanisms (polarization, cake formation, and adsorption). The contribution of the reversible and the irreversible fouling resistances for the microfiltration and ultrafiltration of biological suspensions and the influence of operating parameters on the resistances was previously analyzed by Choi et al. [28]. Li et al. [29] have associated the reversible fouling resistance component to the polarization resistance and the cake resistance and the irreversible fouling resistance component to internal fouling for the ceramic filtration of soy sauce. These two previous studies were limited to steady-state conditions and did not present transient variation of the fouling resistances.

The local and spatial variation of the reversible and irreversible fouling resistance components in the proposed model was developed as follows. The reversible fouling component was assumed to consist predominantly of the polarization resistance and increases due to the cake growth and its associated resistance (Li et al. [29], Choi et al. [28]). Due to the rapid formation of the polarization layer [30,31], the initial reversible resistance $R_{R\,initial}$ was considered to be the resistance of the initial polarization layer.

Experimental results, reported in the next sections, indicated that the initial reversible resistance, $R_{R\,initial}$, increased with increasing TMP and the relationship between $R_{R\,initial}$ and TMP was linear within the range of 27.5 and 55 kPa. A similar relationship between polarization resistance and TMP was shown appropriate for the ultrafiltration of soy protein extracts (Kumar [16]) and the ultrafiltration of soy sauce (Li et al. [29]) and Tu et al. [4] for filtration of organic matter. We combined these experimental results of the initial reversible resistance with the prior knowledge that polarization layer depends on axial position. Instead of TMP, the local pressure drop at a given position along the fiber at $t = 0$ ($\Delta P(z,0)$) was considered in the representation of the initial reversible fouling resistance:

$$R_R(t=0) = R_{R\,initial} = \beta\,(1 + \lambda \times \Delta P(z,0)) \tag{12}$$

The parameters β and λ (Table 2) were obtained experimentally (see Section 3.3 for details).

The transient reversible resistance also depends on the axial position with the dynamics of the reversible resistance where the predominant mechanism is cake formation. During the phase of cake formation, the increase of the cake resistance depends on the permeate velocity and protein concentration [21]. In the proposed model, the reversible resistance rate was assumed proportional to the local permeate velocity, $v_w(z,t)$, and the local protein concentration at the membrane surface at a given position along the fiber, $C_w(z,t)$

$$\frac{dR_R(z,t)}{dt} = \frac{v_w(z,t)C_w(z,t)}{k_R} \tag{13}$$

The parameter k_R was obtained by minimizing the error between the prediction and the experimental data for the permeate flux and the protein concentration at TMP = 34.5 kPa. Experimental results obtained at TMP = 41.5 kPa for the non-electroacidified soy protein extract served for the model validation.

The irreversible resistance refers to the protein adsorption and depends primarily on the physicochemical properties of the membrane and the soy protein extracts (ionic strength, pH) rather than the hydrodynamics of the process [32]. The irreversible steady-state resistance, $R_{I\,ss}$, corresponds to the situation where after a given time, no experimental variation was detected and was considered as steady-state. Previous studies for BSA indicate that the protein adsorption on the membrane surface reaches a plateau with time. Matthiasson [33] filtered BSA solutions with a dead-end membrane system and observed that the adsorption of BSA had already reached a plateau after 10 min. Turker et al. [34] investigated BSA adsorption on hollow fiber membrane surface and observed an equilibrium after 20 min. Based on these observations, the dynamics of the irreversible fouling resistance were assumed to be first-order (Eq. (14)) with an apparent time constant τ_I that depends on the protein concentration at the membrane surface and the initial condition given by Eq. (15)

$$\tau_I \frac{dR_I}{dt} = (R_{I\,ss} - R_I), \qquad \tau_I = \frac{k_I}{C_w(z,t)} \tag{14}$$

$$R_I(t=0) = R_{I\,initial} \tag{15}$$

The initial and steady-state irreversible fouling resistances, $R_{I\,initial}$ and $R_{I\,ss}$, were measured experimentally (Section 3.3) and were directly used in the computational model. The time constant parameters k_I was obtained as for k_R. Fig. 3 illustrates a summary of the model developed in the current study.

2.7. Mesh geometry

A non-uniform triangular mesh was adopted with the mesh density being higher near the membrane surface. Subramani et al. [7], Huang and Morrissey [9] and Marcos et al. [11] used a similar approach. The specified maximum size of element and the growth rate of the elements controlled the automatic meshing on the membrane boundary. Different mesh resolutions, 1247, 1773, 2021, and 2405, were considered to identify the mesh dependency of the model. The protein concentration along the radius of the fiber at the half length of the fiber ($z = 0.15$ m) was plotted for each mesh resolution and percent error at each element was calculated with Eq. (16). The mesh refinement was stopped when a 0.1% average

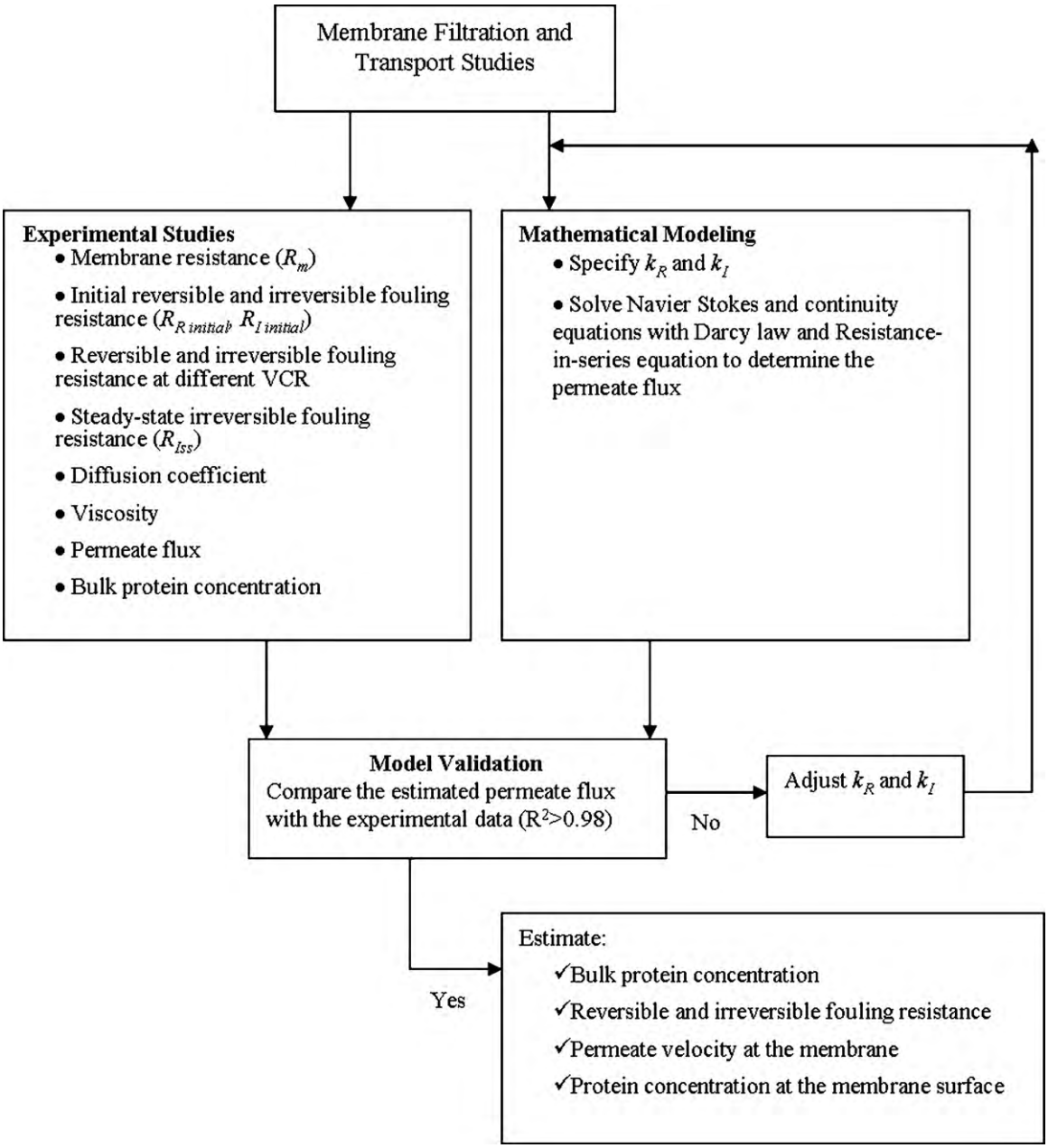

Fig. 3. Methodology for model development and validation.

error was reached

$$\text{Error}\,(\%) = \left| \frac{\text{protein concentration}_{\text{small mesh size}} - \text{protein concentration}_{\text{large mesh size}}}{\text{protein concentration}_{\text{smaller mesh size}}} \right| \times 100 \qquad (16)$$

Finally, a mesh resolution of 2021 with 15 cells along the symmetry line, 17 cells across the half of the channel, and 120 cells for the membrane was chosen. The solution to the numerical problem was also obtained with quadrilateral mesh elements. The results were compared with the triangular mesh elements and no significant differences were observed.

2.8. Numerical solution

CFD tools use finite element method or finite volume method. For membrane filtration, the two methods have been used. For instance, Subramani [7], Huang [9] and Ma [13] used finite element methods to simulate the velocity and the concentration in the membrane system. The momentum equation is not difficult to be solved under laminar conditions. The diffusion convection equation (protein concentration in this study) may present potential difficulties for the finite element method and the finite volume method. The large concentration gradient near the membrane and the large Peclet number in the same region cause challenges for the accuracy and the artificial diffusion. The use of specific numerical schemes (UPwind Petrov Galerkine) and a fine meshing addressed these issues; these features are available in COMSOL and were used in this study. The commercially available finite element code, COMSOL Multiphysics (version 3.5), was used to solve the governing equations. According to the finite element principles, COMSOL Multiphysics converts the partial differential equations of the model

(strong form) to the weak form by multiplying the model equations with a test function, followed by integration which involves integration by parts of the flux term at the boundary. After the finite element discretization, a set of differential algebraic equations was obtained and solved by a variable step-size backward differentiation formula (BDF). The BDF order is variable and ranges between 1 and 5. The direct solver, UMFPACK, was used to solve the resulting linear system. UMFPACK solves linear systems with the nonsymmetric-pattern multifrontal method and direct LU factorization of the sparse matrix. The ordinary differential equations describing the resistance dynamics were introduced with the weak formulation (related to the mathematical weak form) on the boundary of the domain. The ordinary differential equations describing the tank dynamics were solved with a Runge Kutta method provided by COMSOL. For the cylindrical geometry investigated in this study, a validation was performed with the approximated analytical solution (Yuan's solution) for Navier–Stokes equation and a porous wall. Very good agreement was obtained (data not shown) demonstrating that the CFD numerical tool is adequate. A Pentium 2.13 GHz with 2 GB of Ram was used for the numerical tests. The simulations were assumed to converge when the weighted absolute residual norm was less than 10^{-5}.

3. Experimental

3.1. Materials and methods

Electroacidified and non-electroacidified soy protein extracts, containing approximately 60% (w/w) protein, 30% (w/w) carbohydrates, and 10% (w/w) ash, were provided by Agriculture and Agri-Food Canada (Saint-Hyacinthe, QC, Canada). A 2% (w/w) soy protein extract solution was prepared by mixing a preweighed amount of SPE powder with Nanopure water (resistivity > 17.5 MΩ-cm) and was stirred at room temperature for 1 h to allow rehydration. The suspension was then centrifuged at 10,000 RPM for 17 min at 23 °C using a Beckman Coulter L7-35 ultracentrifuge (Mississauga, ON, Canada) to remove any insoluble components. The supernatant was used as the feed solution for the ultrafiltration concentration experiments. The initial protein concentration in the feed solution was 10 g/L for all experiments.

3.2. Experimental setup

The details of the experimental set-up are given in Ref. [18]. Briefly summarized, a polysulfone hollow fiber membrane module (GE Healthcare, Baie D'Urfe, QC, Canada) with a nominal molecular weight cutoff (MWCO) of 100 kDa was used in this work. The feed was pumped with a progressing cavity pump (Moyno Inc, Springfield, OH), and the flow rate was measured by a flowmeter. The pressure was monitored at the feed and the retentate side with two pressure transducers. The transmembrane pressure (TMP) was controlled on the retentate side by a manual pinch valve. The flowmeter, pressure transducers and manual pinch valve were purchased from Cole Parmer Canada Inc. (Anjou, QC, Canada). The permeate was collected in a reservoir, and its mass measured with a balance (Ohaus Corp., Pine Brooks, NJ, USA) and monitored by Labview 7.1 data acquisition system. The permeate flux was measured by weighing the permeate at specified time intervals. All the experiments were performed at 25 ± 1 °C. The clean membrane resistance was estimated before each experiment with Darcy's law and ΔP = TMP in Eq. (10), for different TMP.

3.3. Initial fouling resistance estimation

The first sets of experiments were performed to analyze the fouling mechanisms at the beginning of the filtration. The filtration, performed at different TMP for both electroacidified and non-electroacidified soy protein extracts, was stopped after 2 min to measure the reversible and irreversible fouling resistances. After the 2-min filtration period, the membrane was rinsed with 1L Nanopure water in both non-recycle and total recycle mode at the same operating conditions as the filtration. The water flux was then measured and used to estimate the initial irreversible resistance ($R_{I\,initial}$). The initial reversible resistance ($R_{R\,initial}$) was calculated by subtracting the sum of the clean membrane resistance and the initial irreversible resistance from the global resistance (Eq. (10)). The experimental values of $R_{I\,initial}$ and $R_{R\,initial}$ were directly used in the computational model as the initial conditions for the filtration.

3.4. Transient reversible (R_R) and irreversible (R_I) resistances estimation

To understand how the reversible and irreversible fouling resistances change during the concentration, filtrations were conducted at a number of specified VCR and a constant TMP to measure the reversible and irreversible fouling. The volume concentration ratio (VCR) is the extent of volume reduction during the filtration operation and is defined by Eq. (17)

$$\mathrm{VCR} = \frac{V_{feed}}{V_{feed} - V_{permeate}} \tag{17}$$

where V_{feed} and $V_{permeate}$ are the volume of the feed and permeate, respectively. $V_{permeate}$ is calculated by integrating Q_{per} over time.

The reversible and irreversible fouling resistances were measured at the end of the filtration as described in the previous section and were then compared with the results obtained from the CFD model.

3.5. Protein quantification

Protein concentration in the retentate was analyzed according to the Bradford assay (Standard Procedure for Microtiter Plates, Bio-Rad Laboratories, Mississauga, ON, Canada) with lyophilized bovine serum albumin (Bio-Rad Laboratories, #500-0007) as standard. Absorbance was read at 590 nm in the Multiskan Ascent microtiter plate reader (Labsystems, Helsinki, Finland).

4. Results and discussion

4.1. Experimental fouling observations

The first step for the model development was to characterize experimentally the fouling resistances for the initial conditions and as the concentration operation proceeded. The initial fouling resistances, measured experimentally after 2 min of concentration operation and distinguished as reversible fouling resistance (removed by water wash) and irreversible fouling resistance (removed by chemical cleaning), are presented in Fig. 4. The initial irreversible fouling resistance for the electroacidified soy protein extract is double that of the non-electroacidified soy protein extract while the reversible fouling resistance is similar. The higher initial irreversible fouling resistance observed for the electroacidified soy protein extract suggests more significant protein-membrane interactions at pH 6, pH conditions closer to the soy protein isoelectric point (4.8–5.2). These pH conditions represent lower electrostatic repulsion forces than for the non-electroacidified soy protein extract at pH 9. Also, the presence of quantifiable irreversible fouling resistance for both extracts can explain the observations previously reported for the discontinuous diafiltration approach, a dilution of the concentrated retentate solution after an initial concentration step, which was unable to improve the permeate flux for both the non-electroacidified and electroacidified

Table 3
Contribution of reversible and irreversible fouling during soy protein concentration by cross-flow ultrafiltration at TMP = 34.5 kPa.

VCR	Non-electroacidified soy protein extract				Electroacidified soy protein extract			
	Reversible fouling resistance, R_R [m^{-1}]		Irreversible fouling resistance, R_I [m^{-1}]		Reversible fouling resistance, R_R [m^{-1}]		Irreversible fouling resistance, R_I [m^{-1}]	
	Exp	Model	Exp	Model	Exp	Model	Exp	Model
1[a]	2.85×10^{12}	2.67×10^{12}	5.8×10^{11}	–	2.27×10^{12}	–	1.31×10^{12}	–
2	3.9×10^{12}	3.57×10^{12}	1.62×10^{12}	1.78×10^{12}	5.5×10^{12}	4.78×10^{12}	3.47×10^{12}	3.80×10^{12}
2.4	–	–	–	–	–	5.19×10^{12}	3.92×10^{12}	3.93×10^{12}
3	5.2×10^{12}	3.99×10^{12}	1.92×10^{12}	1.93×10^{12}	–	–	–	–
3.3	–	–	–	–	7.4×10^{12}	5.89×10^{12}	4.17×10^{12}	4.07×10^{12}
4	5.28×10^{12}	4.26×10^{12}	2.03×10^{12}	1.97×10^{12}	–	–	–	–

[a] Estimated after 2 min of filtration. The experimental values of the initial fouling were directly imported to the model, as is explained in the text.

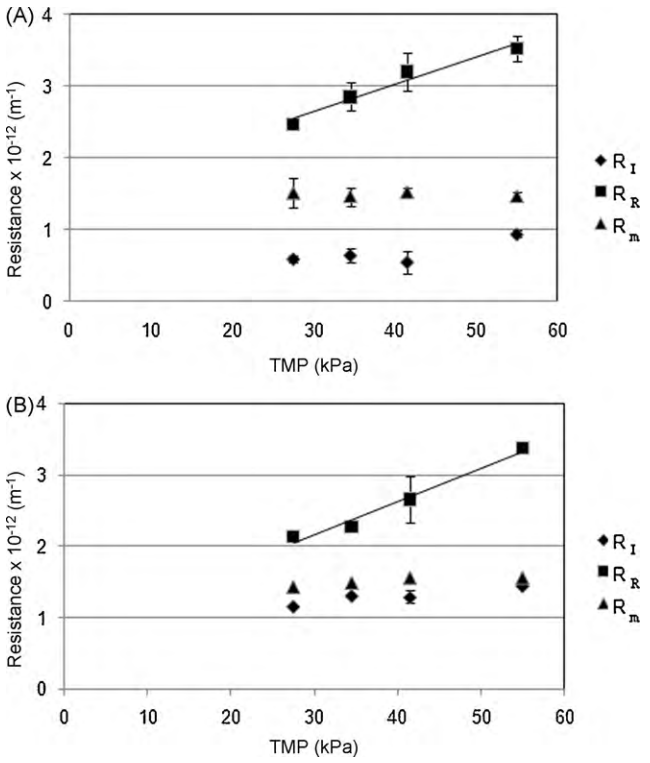

Fig. 4. Effect of TMP on the initial fouling; axial velocity = 1 m s^{-1}; (A) non-electroacidified soy protein extract; (B) electroacidified soy protein extract (mean ± SD, $n = 2$). Solid line shows the fit based on Eq. (13) and parameters Table 2.

soy protein extracts [17]. As expected, the TMP affected mainly the initial reversible fouling resistance that increases with increasing TMP. Based on these observations, the effect of TMP on the initial reversible fouling resistance for the model development was represented with a linear relationship in Eq. (12) and with the parameters presented in Table 2. The initial reversible fouling resistances for the non-electroacidified soy protein extract are slightly greater than those of the electroacidified soy protein extract.

The second step was to validate the transient resistance model estimates with independent experimental data obtained for the entire concentration operation. Table 3 presents model and experimental fouling resistances at different VCR conditions. In general, there is a good agreement between experimental and model estimates. The reversible fouling resistances are quite similar for both extracts. In contrast, the irreversible fouling resistances are more significant for the electroacidified extract. The irreversible fouling resistance increases initially with a subsequent leveling off observed for both the non-electroacidified and the electroacidified soy protein extracts. This behavior was estimated by Eq. (14) and the parameters presented in Table 2. In contrast, the reversible fouling resistance increases as long as the filtration operation continues as represented by Eq. (13). The increase is more pronounced for the electroacidified soy protein extract. For example, at VCR = 3, the reversible fouling resistance of the non-electroacidified soy protein extract has doubled while for the electroacidified soy protein extract it has tripled. It appears that pH has an effect on the formation of the reversible fouling resistance related to the formation of the concentration polarization layer. The lower pH of the electroacidified soy protein extract allows proteins to come into closer contact forming a denser concentration polarization layer [15].

4.2. Permeate flux and protein concentration modeling

The permeate flux during the entire concentration operation was modeled for different conditions of inlet axial velocity and

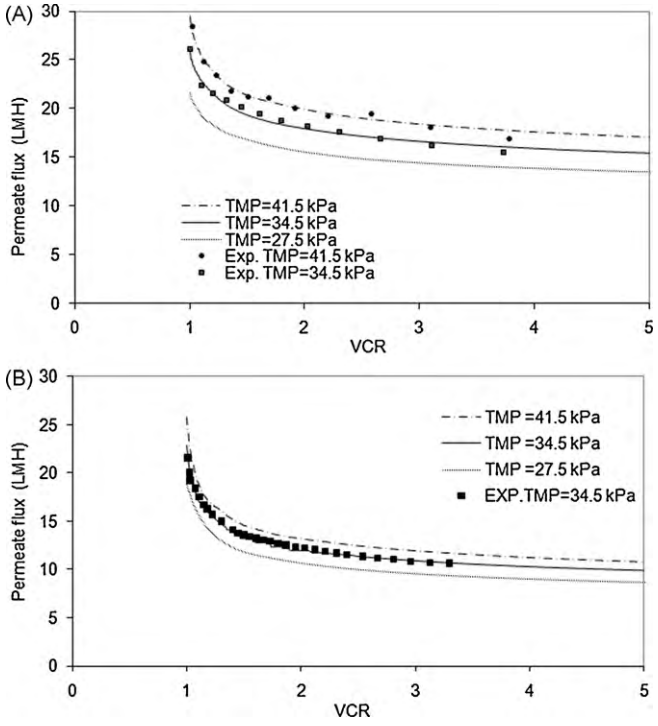

Fig. 5. Effect of TMP on the permeate flux; axial velocity = 1 m s^{-1}; (A) non-electroacidified soy protein extract; (B) electroacidified soy protein extract.

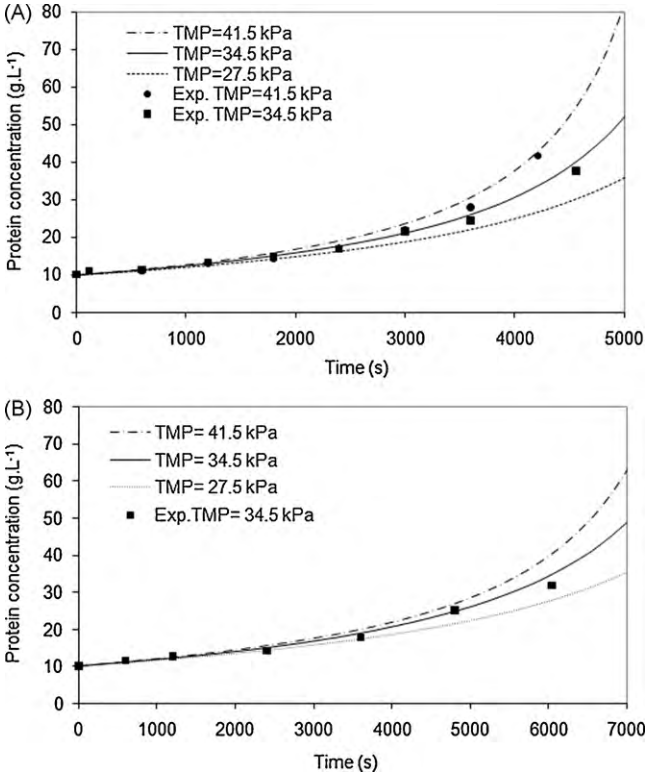

Fig. 6. Effect of TMP on the bulk protein concentration; axial velocity = 1 m s^{-1}; (A) non-electroacidified soy protein extract; (B) electroacidified soy protein extract.

TMP and two types of soy protein extracts. The model incorporated the behavior of the initial and steady-state irreversible fouling resistances deduced from experiments. The model contained two adjustable parameters, k_R, k_I (Table 2) estimated by minimizing the error between the prediction and the experimental data for the permeate flux and the protein concentration at one TMP (34.5 kPa). There is a very good agreement between the model and the experimental data for the permeate flux (Fig. 5) and the protein concentration in the retentate (Fig. 6). The model validation also shows a good agreement between model estimates and experimental data for the permeate flux and the protein concentration of the non-electroacidified soy protein extract at a different TMP (41.5 kPa) (Figs. 5A and 6A). The effect of electroacidification pretreatment on the permeate flux and protein concentration (Figs. 5 and 6) is also well captured by the model. The estimates of the individual contribution of the reversible and the irreversible fouling resistances at different concentration conditions (VCR) corresponding to independent experiments for the non-electroacidified and electroacidified soy protein extract (Table 3) are also very good and demonstrates the applicability and ability of the CFD model to provide insights on the fouling mechanisms. Experimental and model estimates indicate that the reversible resistance is always higher than the irreversible resistance for the electroacidified and non-electroacidified soy protein extract. The difference is less pronounced for the electroacidified soy protein extract. The more significant reversible fouling resistance in comparison to the irreversible fouling resistance agrees with the observation made by Li et al. [29] for the microfiltration of raw soy sauce. Note that this model was able to estimate appropriately the magnitude of the two fouling resistance components and their transient behavior. Recent models have difficulty to evaluate accurately the balance between the different resistances. For instance, the model of Schausberger et al. [14] underestimated the polarization resistance and overestimated the adsorption resistance (with respect to their experimental measurements).

The model provides information on the two important operating parameters, TMP and inlet axial velocity. Increasing the TMP from 27.5 to 41.5 kPa, improved the permeate flux during the entire concentration operation for both types of soy protein extracts. As the permeate flux is inversely proportional to the global fouling resistance (Eq. (10)), a significant global resistance corresponds to a low permeate flux. The simulated results at VCR = 5 show a more pronounced effect of the TMP on the total fouling resistance ($R_R + R_I$) for the non-electroacidified soy protein extract, 7.20×10^{12}, 6.46×10^{12}, and 5.79×10^{12} m^{-1} at TMP of 41.5, 34.5, and 27.5 kPa, respectively in comparison with the electroacidified soy protein extract, 1.22×10^{13}, 1.09×10^{13} and 9.54×10^{12} m^{-1} at TMP of 41.5, 34.5, and 27.5 kPa, respectively. The effect of the TMP on the protein concentration was less pronounced but became more important only after 3000 s. The model estimates indicate that increasing the inlet axial velocities from 0.5 to 1.5 m s^{-1} reduces more significantly the filtration time to reach VCR = 5 for the electroacidified soy protein extract (8100 and 6840 s) compared to the non-electroacidified protein extract (5430 and 4890 s) as shown in Fig. 7. The limited effect of the inlet axial velocity to improve the permeate flux supports the experimental observations where a significant irreversible fouling was already observed after 2 min of the concentration operation. A consequence of the limited effect of increasing axial velocity is reflected in the very small differences for the protein concentration in the retentate for different axial velocities (Fig. 8).

4.3. Effect of electroacidification on the fouling behavior

The CFD model, developed in this study and based on the dynamics of the reversible and irreversible fouling resistances specific to each soy protein extract (Eqs. (13) and (14)), provided spatial information on the axial fouling behavior, i.e. along the length of the fiber as the concentration operation proceeded (Figs. 9 and 10). Differ-

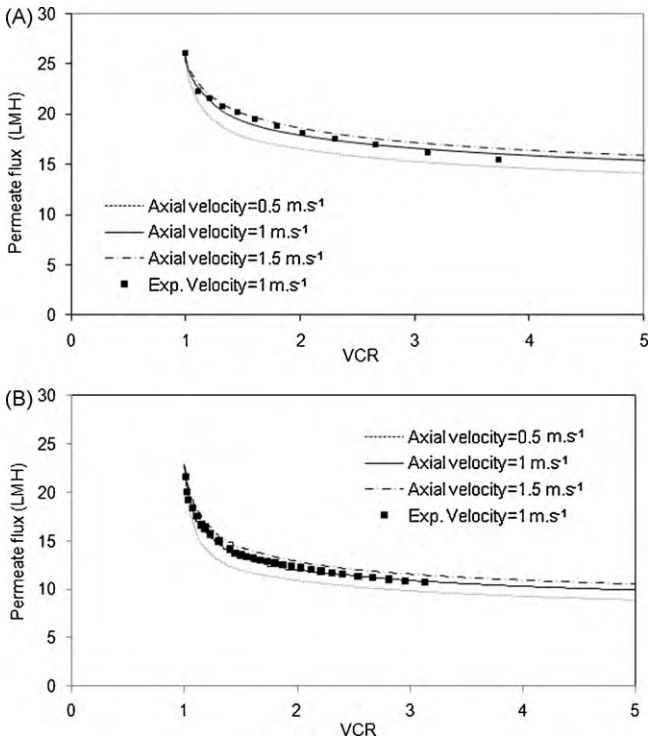

Fig. 7. Effect of axial velocity on the permeate flux; TMP = 34.5 kPa; (A) non-electroacidified soy protein extract; (B) electroacidified soy protein extract.

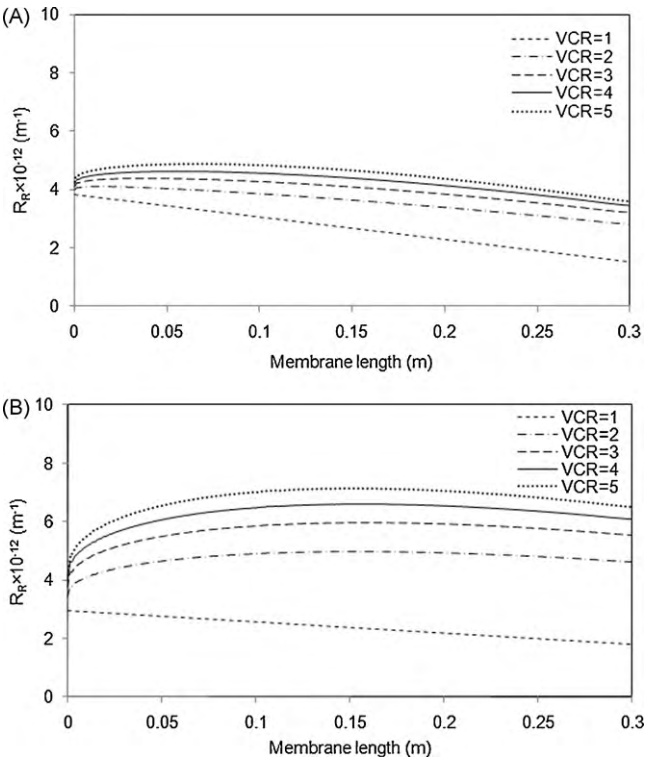

Fig. 9. Effect of VCR on the estimated reversible fouling resistance; TMP = 34.5 kPa; axial velocity = 1 m s^{-1}; (A) non-electroacidified soy protein extract; (B) electroacidified soy protein extract.

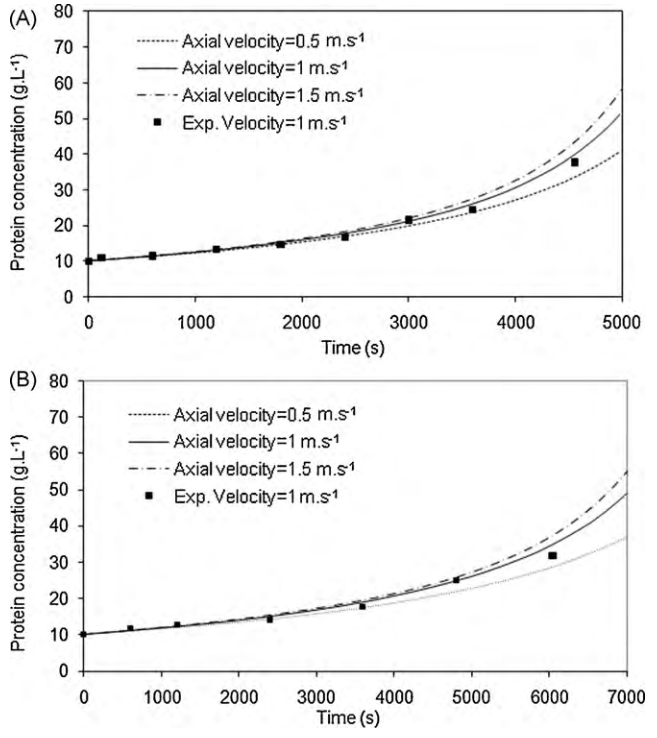

Fig. 8. Effect of axial velocity on the bulk protein concentration; TMP = 34.5 kPa; (A) non-electroacidified soy protein extract; (B) electroacidified soy protein extract.

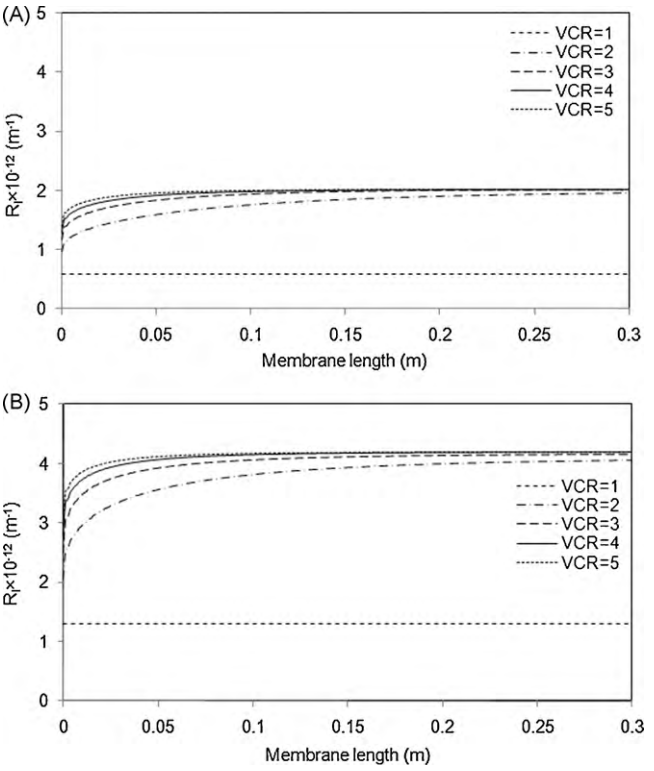

Fig. 10. Effect of VCR on the estimated irreversible fouling resistance; TMP = 34.5 kPa; axial velocity = 1 m s^{-1}; (A) non-electroacidified soy protein extract; (B) electroacidified soy protein extract.

Table 4
Model estimates of the maximum reversible fouling resistance during soy protein concentration by cross-flow ultrafiltration at TMP = 34.5 kPa and axial velocity = 1 m s^{-1}.

VCR	Non-electroacidified soy protein extract		Electroacidified soy protein extract	
	Estimated maximum reversible fouling resistance, R_R [m^{-1}]	Position [m]	Estimated maximum reversible fouling resistance, R_R [m^{-1}]	Position [m]
1	3.82×10^{12}	0	2.96×10^{12}	0
2	4.10×10^{12}	0.0135	4.98×10^{12}	0.158
3	4.38×10^{12}	0.0387	5.97×10^{12}	0.158
4	4.63×10^{12}	0.06	6.62×10^{12}	0.158
5	4.87×10^{12}	0.0682	7.12×10^{12}	0.149

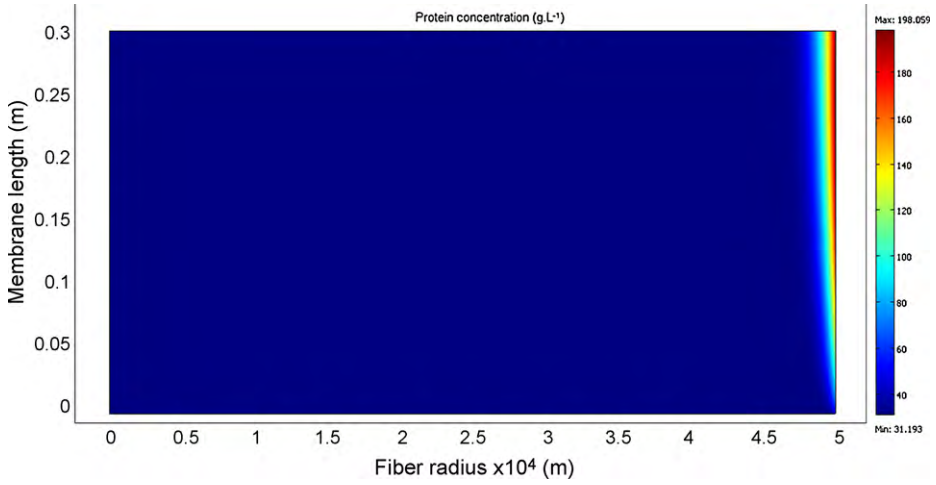

Fig. 11. Estimated protein concentration profile inside the fiber, TMP = 34.5 kPa; axial velocity = 1 m s^{-1}; t = 4020 s; non-electroacidified soy protein extract.

ences were observed according to the type of soy protein extract and the type of fouling resistance. The simulated reversible fouling resistance profile reached a maximum before the end of the fiber, which is more pronounced for the electroacidified soy protein extract and at higher VCR (Table 4). As VCR increases, the estimated reversible fouling resistance increases more significantly for the electroacidified soy protein extract. The reversible fouling resistance is related to the profile along the fiber of the permeate flux and the protein concentration at the membrane surface, which will be discussed in the next section. The simulated irreversible fouling resistance profile is very different. As shown in Fig. 10, a sharp increase at the entrance of the fiber is predicted with a subsequent relatively constant value for the remaining fiber length. The initial sharp increase could be related to the concentration boundary layer that was not fully developed (Fig. 11). The initial sharp increase was more pronounced for the electroacidified soy protein extract. For VCR = 3 and higher, the irreversible fouling resistance did not vary very much and seemed to reach a plateau and this behavior was observed previously [33,34].

As noted, the fouling behavior is different between the electroacidified and non-electroacidified soy protein extracts. The differences come from the pH effect. According to Marshall et al. [32], the pH affects protein for three reasons: the pH changes the protein conformation and its ability to deposit on the membrane; the pH changes the size of the protein or the size of protein aggregates; the pH changes the charge between the membrane and the protein. For soy protein extracts, previous studies reported size and charge differences according to electroacidification conditions. Mondor et al. [19] reported a larger mean particle diameter for the electroacidified soy protein extract at pH 6 reconstituted in water compared with the non-electroacidified soy protein at pH 9 and Skorepova and Moresoli [17] reported reduced interactions between proteins having a reduced negative charge for the electroacidified soy protein extracts and cations (minerals and phytic acids). In the context of fouling, the reduced negative charge and the larger diameter for the electroacidified soy protein extract could be associated with a more important protein adsorption and the more severe irreversible fouling observed experimentally in this study for the soy protein extracts subjected to electroacidification.

4.4. Protein concentration and velocity profile inside the membrane fiber

The estimated spatial protein concentration inside the fiber at VCR = 3 for non-electroacidified soy protein extract (Fig. 11) presents a uniform protein concentration profile along the fiber length and away from the membrane surface confirming that the bulk protein concentration does not change significantly along the fiber. This uniform bulk protein concentration can be explained by the small permeate velocity compared to the axial velocity. The thickness of the concentration boundary layer increases along the fiber length but represents less than 10% of the fiber radius. The

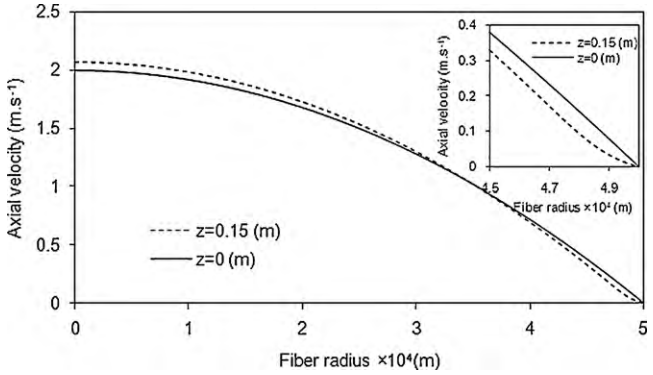

Fig. 12. Estimated axial velocity profile along the fiber radius, TMP = 34.5 kPa; axial velocity = 1 m s^{-1}; t = 4020 s; non-electroacidified soy protein extract. Insert shows the profile near the membrane surface.

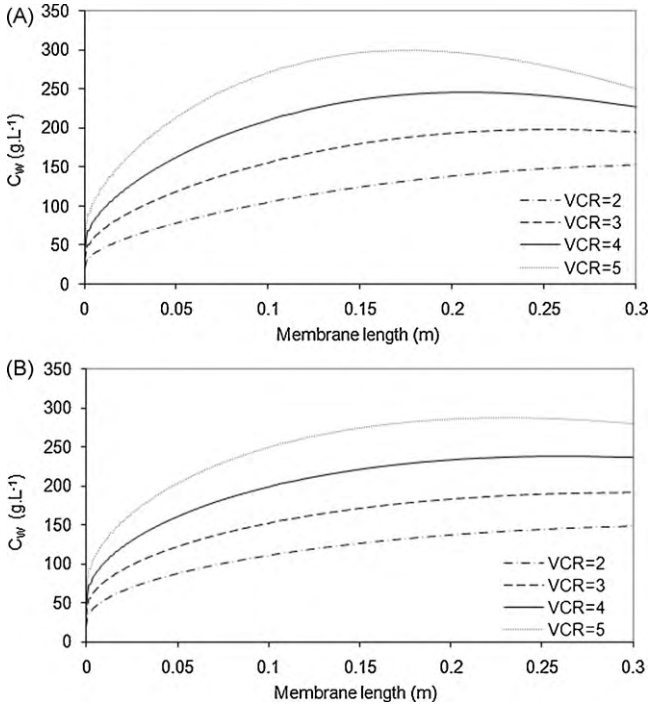

Fig. 13. Effect of VCR on the estimated protein concentration at the membrane surface; TMP = 34.5 kPa; axial velocity = 1 m s^{-1}; (A) non-electroacidified soy protein extract; (B) electroacidified soy protein extract.

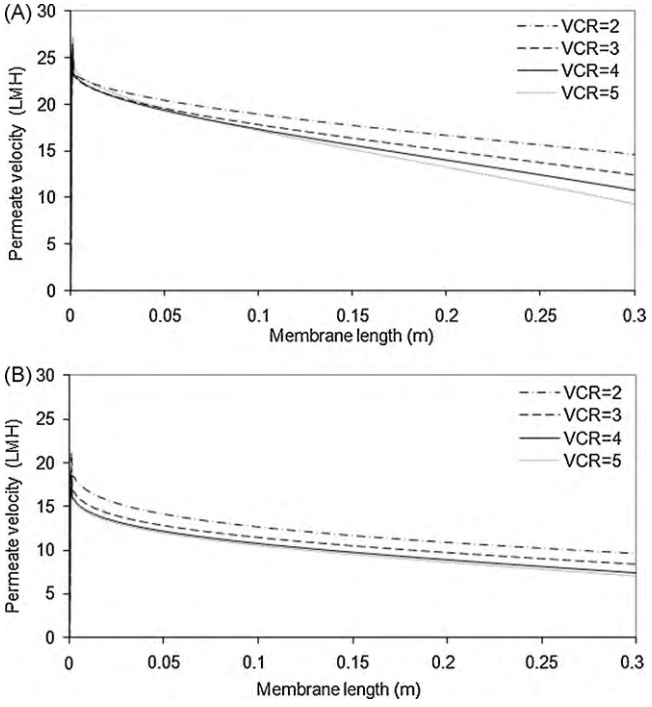

Fig. 14. Effect of VCR on the estimated permeate velocity at the membrane surface; TMP = 34.5 kPa; axial velocity = 1 m s^{-1}; (A) non-electroacidified soy protein extract; (B) electroacidified soy protein extract.

axial velocity profile (Fig. 12) corresponds to the classical parabolic profile for laminar flow. It shows that the axial velocity inside the fiber is affected by the permeate velocity and the concentration boundary layer on the membrane surface as shown in the close-up of the membrane surface where a different profile is observed according to position along the fiber.

Since the fouling is determined by the conditions near the membrane surface, it is important to analyze the protein concentration at the membrane surface ($C_w(z, t)$) and the permeate velocity ($v_w(z, t)$). The estimated protein concentration at the membrane surface increased significantly along the fiber length as concentration proceeded, i.e. increasing VCR (Fig. 13) for both extracts. The position and the magnitude of the maximum are different according to VCR and type of soy protein extract. As the protein concentration at the membrane surface is related to the reversible fouling resistance according to Eq. (13), their differences are interrelated. The estimate of the average protein concentration at the membrane surface, for the non-electroacidified and electroacidified soy protein extract are 116 and 118 g/L at VCR = 2 and then increases to 258 and 250 g/L at VCR 5. These values have the same order of magnitude as those found in Ref. [16] for soy protein concentrate. A predicted maximum protein concentration at the membrane surface before the exit of the membrane was also reported by Marcos et al. [11] for soy protein extracts and Ma et al. [13] for dextran solutions and was explained by a variable permeate velocity as considered in the current study. Fig. 14 presents the estimated axial permeate velocity at the membrane surface. A decreasing local permeate velocity is predicted along the fiber length for both types of extracts. The decrease is linear at the beginning of the filtration (VCR = 1, data not shown) because of the decreasing local transmembrane pressure along the fiber (associated with the pressure drop inside the fiber). The decrease is more pronounced as the VCR increases and is more significant for the electroacidified soy protein extract. A non-linear axial velocity decrease was also predicted by Ma et al. [13] for dextran solutions when a variable viscosity was considered. Marcos et al. [11]

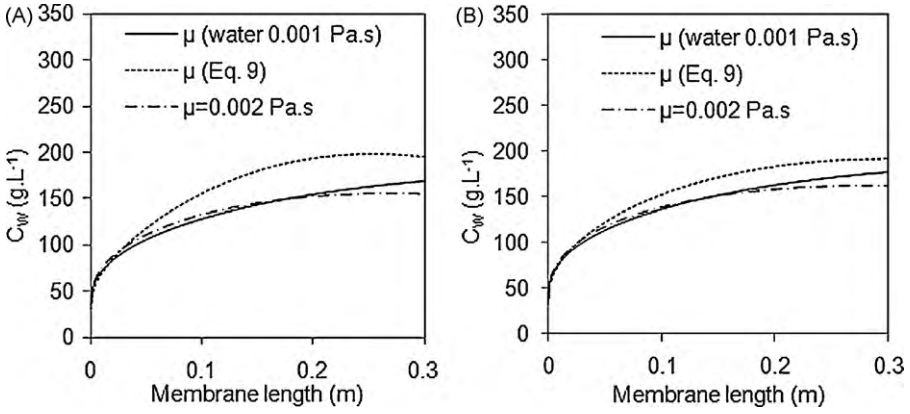

Fig. 15. Effect of viscosity on the estimated protein concentration at the membrane surface; TMP = 34.5 kPa; axial velocity = 1 m s^{-1}; VCR = 3; (A) non-electroacidified soy protein extract; (B) electroacidified soy protein extract.

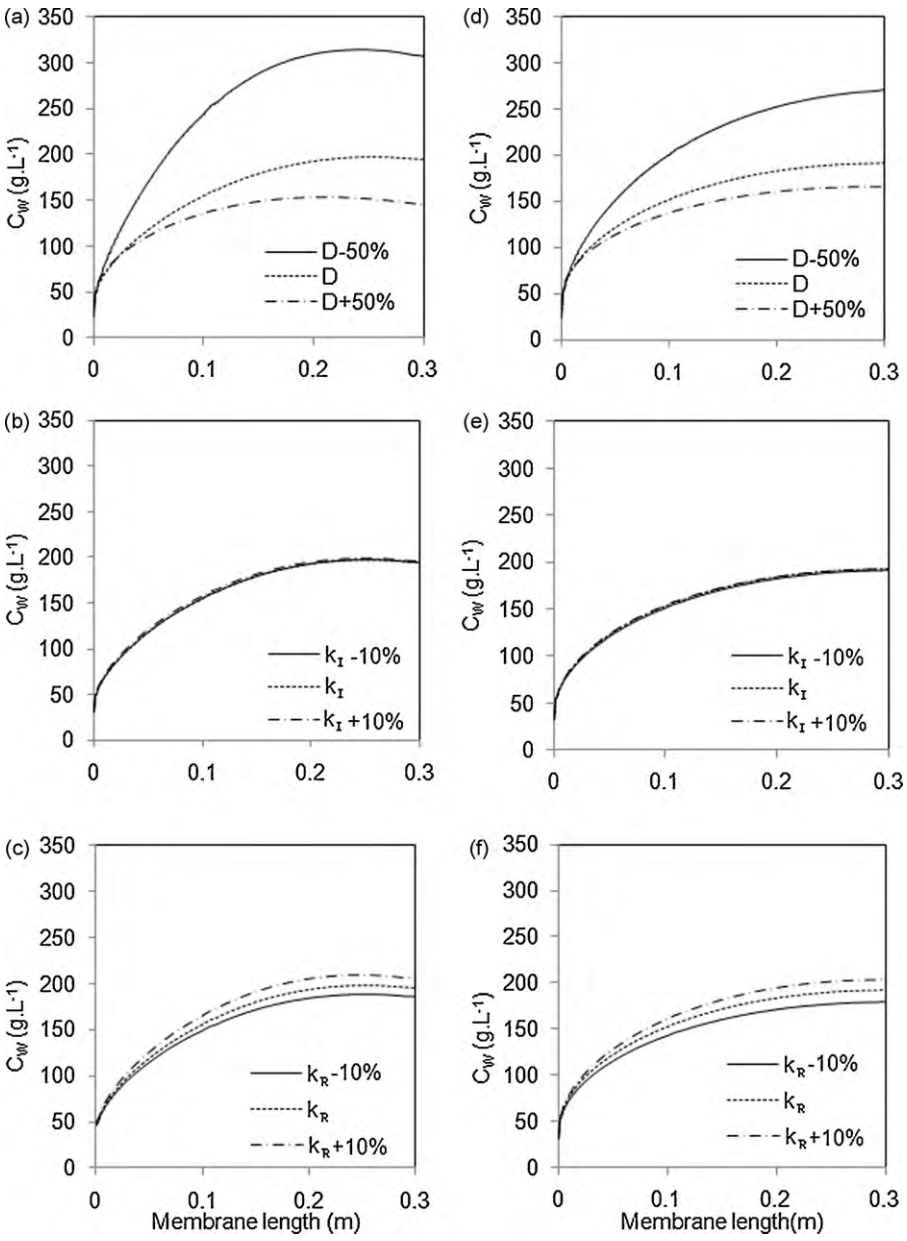

Fig. 16. Model sensitivity analysis for the estimated protein concentration at the membrane surface of the non-electroacidified (a–c) and electroacidified (d–f) soy protein extract; TMP = 34.5 kPa; axial velocity = 1 m s^{-1}; VCR = 3 (t = 4020 s).

reported a linear decrease as the concentration proceeded for non-electroacidified soy protein extracts. The viscosity relationship may explain the different predictions between our results and those reported by Marcos et al. [11].

4.5. Effect of viscosity

UF is a pressure driven process in which the pressure drop along the fiber and the transmembrane pressure play an important role in the fouling behavior. During the filtration, the protein concentration increases in the retentate and consequently the viscosity of the solution (Eq. (9)). As the viscosity increases, the pressure drop will also increase. The effect of the viscosity on the estimated C_w is significant (Fig. 15). When a low and constant viscosity (water) is considered, the protein concentration at the membrane surface increases along the fiber such that the maximum is observed at the end of the fiber. However, when a high viscosity with a protein concentration dependency is considered (Eq. (9)), the maximum protein concentration at the membrane surface increases for both extracts and occurs before the exit of the fiber for the non-electroacidified soy protein extract. The critical viscosity, corresponding to the maximum protein concentration at the membrane surface is 0.002 Pa s. Increasing the viscosity from 0.001 Pa s (water) to 0.002 Pa s is associated with a negligible increase of the average total fouling ($R_r + R_I$) at VCR = 3 (0.07% for the non-electroacidified and 0.6% for the electroacidified soy protein extracts). A more significant increase of the total fouling, 5%, was estimated for both non-electroacidified and electroacidified soy protein extract when the constant value of 0.001 Pa s for the viscosity was replaced by the concentration dependent viscosity (Eq. (9)). This shows the importance of having the appropriate viscosity relationship with the contribution of the protein concentration and the effect of electroacidification.

4.6. Model sensitivity analysis

Three parameters were selected to perform the model sensitivity analysis: the diffusivity coefficient, the parameter k_R (Eq. (13)), and the parameter k_I (Eq. (14)). The diffusivity coefficient was changed by ±50% and selected according to previous studies for BSA where the diffusion coefficient varies by about 50% when the concentration is multiplied by 10 (Keller et al. [35]). The parameters k_R and k_I were changed by ±10%. The protein concentration at the membrane surface (C_w) was chosen to evaluate the influence of the three selected parameters because it represents a local variable and has a very important role in the fouling dynamics. The effects of the different parameters were investigated for VCR = 3 and are reported for the non-electroacidified soy protein extract (Fig. 16a–c) and for the electroacidified soy protein extract (Fig. 16d–f).

The effect on the protein concentration at the membrane surface (Fig. 16a and d) when the diffusion coefficient decreases by 50% resulted in 52% and 32% increase for the non-electroacidified and electroacidified soy protein extract, respectively. In contrast, the effect of a 50% increase for the diffusion coefficient resulted in 15% and 11% decrease of the protein concentration at the membrane surface for non-electroacidified and electroacidified soy protein extract, respectively. These estimates indicate that the protein concentration at the membrane surface is much more sensitive to the diffusion coefficient for the non-electroacidified soy protein suggesting that back transport associated with the diffusion coefficient plays a more important role.

A 10% increase in the irreversible fouling parameter, k_I shown in Fig. 16b and e, results in a negligible increase of the protein concentration at the membrane surface (1%). Increasing by 10% the reversible fouling resistance parameter, k_R, increases the protein concentration at the membrane surface by 4.6% for both the non-electroacidified soy protein extract and the electroacidified soy protein extract (Fig. 16c and f). Increasing the parameters k_R and k_I decrease the rate of growth of the fouling resistance that eventually increases the convective protein flux and the resulting protein concentration at the membrane surface.

5. Conclusion

Computational fluid dynamics (CFD) provided an attractive tool for the modeling of the complete sequence, feed tank and hollow fiber ultrafiltration unit. A model was developed to investigate the transient permeate flux and protein concentration and the spatial fouling behavior during the concentration of soy protein extracts by membrane ultrafiltration and subjected to electroacidification. The CFD model solved the transient Navier–Stokes equations and the continuity equation in 2D cylindrical coordinates. A new transient two-component fouling resistance model based on the local pressure difference, permeate velocity and protein concentration and fitted from experimental data was implemented in the resistance-in-series flux model to describe the dynamics of the reversible and irreversible fouling during the filtration. The concentration dependency of the viscosity of the solution and the effect of electroacidification were considered in the model development and shown to affect significantly the estimated protein concentration at the membrane surface. The model provided an accurate prediction of the experimental permeate flux, the protein concentration and the fouling dynamics during the concentration operation. In particular, the model was able to estimate accurately each of the transient reversible and irreversible fouling resistances and the contribution of electroacidification, a limitation of many models previously published. The model shows a uniform bulk protein concentration along the fiber but spatially non-uniform protein concentration profile near the membrane surface where the concentration gradient is high. The model estimates show that a moderate increase of the permeate velocity can be achieved when increasing the axial velocity. In contrast, increasing the TMP increases more substantially the permeate flux. Experimental results showed that polarization layer is not the only phenomenon affecting the permeate flux decrease at the beginning of the filtration; the irreversible fouling is an important factor to be considered for the concentration of soy protein extracts. The irreversible fouling at the beginning of the filtration contributes to 20% and 40% of the total fouling for non-electroacidified and electroacidified soy protein extracts, respectively. The model estimates suggest that the irreversible fouling is associated with protein adsorption since a plateau is estimated for both types of extracts. Therefore, the improvement of the concentration of soy protein extracts subjected to electroacidification will be achieved by manipulating the interactions leading to irreversible fouling, i.e. between the proteins and the membrane surface. The model sensitivity analysis showed that the viscosity of the soy protein solution is a sensitive parameter and the concentration dependant viscosity changes significantly the profile of the protein concentration at the membrane surface. The concentration at the membrane surface is also much more sensitive to the diffusion coefficient for the non-electroacidified soy protein suggesting that protein back transport associated with the diffusion coefficient plays a more important role. Future work will focus on the interaction between the proteins and the membrane surface as well as the contribution of the minerals in these interactions. This will be achieved by the modeling of multi-component system considering mineral and carbohydrate transport as well as protein adsorption mechanisms. The role of the diffusion coefficient will also be further examined.

Acknowledgements

This work was financially supported by the Natural Sciences and Engineering Research Council of Canada (NSERC). The authors would also like to thank Agriculture and Agri-Food Canada, St Hyacinthe for providing samples for this work.

Nomenclature

C	protein concentration ($kg\,m^{-3}$)
C_w	protein concentration at the membrane surface ($kg\,m^{-3}$)
C_{feed}	feed tank protein concentration ($kg\,m^{-3}$)
D	diffusion coefficient ($m^2\,s^{-1}$)
k_R	reversible resistance coefficient ($kg\,s\,m^{-2}$)
k_I	irreversible resistance coefficient ($kg\,s\,m^{-3}$)
L	fiber length (m)
n	number of fibers in the ultrafiltration module
P	pressure (Pa)
P_{atm}	atmospheric pressure (Pa)
P_{out}	outlet pressure (Pa)
pI	isoelectric point
ΔP	local transmembrane pressure (Pa)
Q_{feed}	feed tank volumetric rate ($m^3\,s^{-1}$)
Q_{hf}	outlet hollow fiber volumetric rate ($m^3\,s^{-1}$)
Q_{per}	permeate flux ($m^3\,s^{-1}$)
r	radial coordinate (m)
R	fiber radius (m)
R_R	reversible resistance (m^{-1})
$R_{R\,initial}$	initial reversible resistance (m^{-1})
R_I	irreversible resistance (m^{-1})
$R_{I\,initial}$	initial irreversible resistance (m^{-1})
$R_{I\,ss}$	steady state irreversible resistance (m^{-1})

R_G	global resistance (m^{-1})
R_m	clean membrane resistance (m^{-1})
t	time (s)
TMP	average transmembrane pressure (Pa)
VCR	volume concentration ratio
V_{feed}	volume of the feed solution (m^3)
$V_{permeate}$	volume of the permeate solution (m^3)
v_w	permeate velocity ($m\,s^{-1}$)
v_r	radial velocity ($m\,s^{-1}$)
v_z	axial velocity ($m\,s^{-1}$)
$v_{z,max}$	maximum axial velocity ($m\,s^{-1}$)
z	axial coordinate (m)
α	viscosity model constant ($m^3\,kg^{-1}$)
β	initial reversible fouling model constant (m^{-1})
λ	initial reversible fouling model constant (Pa^{-1})
μ	viscosity of the soy protein solution (Pa s)
μ^0	viscosity of water (Pa s)
ρ	density ($kg\,m^{-3}$)
τ_I	irreversible apparent time constant (s)

References

[1] A. Berman, Laminar flow in channels with porous walls, J. Appl. Phys. 24 (1953) 1232–1236.
[2] J. Granger, J. Dodds, N. Midoux, Laminar flow in channels with porous walls, Chem. Eng. J. Biochem. Eng. J. 42 (1989) 193–204.
[3] H.M. Yeh, J.H. Dong, M.Y. Shi, Momentum balance analysis of flux and pressure declines in membrane ultrafiltration along tubular modules, J. Membr. Sci. 241 (2004) 335–345.
[4] S. Tu, V. Ravindran, M. Pirbazari, A pore diffusion transport model for forecasting the performance of membrane processes, J. Membr. Sci. 265 (2005) 29–50.
[5] A.R. Secchi, K. Wada, I.C. Tessaro, Simulation of an ultrafiltration process of bovine serum albumin in hollow-fiber membranes, J. Membr. Sci. 160 (1999) 255–265.
[6] Y. Bessiere, D.F. Fletcher, P. Bacchin, Numerical simulation of colloid dead-end filtration: effect of membrane characteristics and operating conditions on matter accumulation, J. Membr. Sci. 313 (2008) 52–59.
[7] A. Subramani, S. Kim, E.M.V. Hoek, Pressure, flow, and concentration profiles in open and spacer-filled membrane channels, J. Membr. Sci. 277 (2006) 7–17.
[8] A. Pak, T. Mohammadi, S.M. Hosseinalipour, V. Allahdini, CFD modeling of porous membranes, Desalination 222 (2008) 482–488.
[9] L. Huang, M.T. Morrissey, Finite element analysis as a tool for crossflow membrane filter simulation, J. Membr. Sci. 155 (1999) 19–30.
[10] D.E. Wiley, D.F. Fletcher, Techniques for computational fluid dynamics modelling of flow in membrane channels, J. Membr. Sci. 211 (2003) 127–137.
[11] B. Marcos, C. Moresoli, J. Skorepova, B. Vaughan, CFD modeling of a transient hollow fiber ultrafiltration system for protein concentration, J. Membr. Sci. 337 (2009) 136–144.
[12] R. Ghidossi, D. Veyret, P. Moulin, Computational fluid dynamics applied to membranes: state of the art and opportunities, Chem. Eng. Process. 45 (2006) 437–454.
[13] S. Ma, S.C. Kassinos, D. Kassinos, Direct simulation of the limiting flux: I. Introduction of the experimental results, J. Membr. Sci. 337 (2009) 81–91.
[14] P. Schausberger, N. Norazman, H. Li, V. Chen, A. Friedl, Simulation of protein ultrafiltration using CFD: comparison of concentration polarization and fouling effects with filtration and protein adsorption experiments, J. Membr. Sci. 337 (2009) 1–8.
[15] M. Cheryan, Ultrafiltration and Microfiltration Handbook, Technomic Pub. Co., Lancaster, PA, 1998.
[16] N.S. Krishna Kumar, M.K. Yea, M. Cheryan, Ultrafiltration of soy protein concentrate: performance and modelling of spiral and tubular polymeric modules, J. Membr. Sci. 244 (2004) 235–242.
[17] J. Skorepova, C. Moresoli, Carbohydrate and mineral removal during the production of low-phytate soy protein isolate by combined electroacidification and high shear tangential flow ultrafiltration, J. Agric. Food Chem. 55 (2007) 5645–5652.
[18] J. Skorepova, Effect of electroacidification on ultrafiltration performance and physicochemical properties of soy protein extracts, PhD Thesis, University of Waterloo, 2007.
[19] M. Mondor, D. Ippersiel, F. Lamarche, J.I. Boye, Effect of electro-acidification treatment and ionic environment on soy protein extract particle size distribution and ultrafiltration permeate flux, J. Membr. Sci. 231 (2004) 169–179.
[20] M. Mondor, D. Ippersiel, F. Lamarche, J.I. Boye, Production of soy protein concentrates using a combination of electroacidification and ultrafiltration, J. Agric. Food Chem. 52 (2004) 6991–6996.
[21] T. Furukawa, K. Kokubo, K. Nakamura, K. Matsumoto, Modeling of the permeate flux decline during MF and UF cross-flow filtration of soy sauce lees, J. Membr. Sci. 322 (2008) 491–502.
[22] K. Damak, A. Ayadi, B. Zeghmati, P. Schmitz, A new Navier–Stokes and Darcy's law combined model for fluid flow in crossflow filtration tubular membranes, Desalination 161 (2004) 67–77.
[23] P. Schmitz, M. Prat, 3-D laminar stationary flow over a porous surface with suction: description at pore level, AIChE J. 41 (1995) 2212–2226.
[24] T.R. Noordman, K. Kooiker, W. Bel, M. Dekker, J.A. Wesselingh, Concentration of aqueous extracts of defatted soy flour by ultrafiltration—effect of suspended particles on the filtration flux, J. Food Eng. 58 (2003) 135–141.
[25] W.R. Bowen, P.M. Williams, The osmotic pressure of electrostatically stabilized colloidal dispersions, J. Colloid Interface Sci. 184 (1996) 241–250.
[26] C.C. Ho, A.L. Zydney, A combined pore blockage and cake filtration model for protein fouling during microfiltration, J. Colloid Interface Sci. 232 (2000) 389–399.
[27] J.E. Kilduff, S. Mattaraj, G. Belfort, Flux decline during nanofiltration of naturally-occurring dissolved organic matter: effects of osmotic pressure, membrane permeability, and cake formation, J. Membr. Sci. 239 (2004) 39–53.
[28] H Choi, K. Zhang, D.D. Dionysiou, D.B. Oerther, G.A. Sorial, Influence of cross-flow velocity on membrane performance during filtration of biological suspension, J. Membr. Sci. 248 (2005) 189–199.
[29] M. Li, Y. Zhao, S. Zhou, W. Xing, F.-S. Wong, Resistance analysis for ceramic membrane microfiltration of raw soy sauce, J. Membr. Sci. 299 (2007) 122–129.
[30] P. Aimar, C. Taddei, J. Lafaille, V. Sanchez, Mass transfer limitations during ultrafiltration of cheese whey with inorganic membranes, J. Membr. Sci. 38 (1988) 203–221.
[31] K.W.K. Yee, D.E. Wiley, J. Bao, A unified model of the time dependence of flux decline for the long-term ultrafiltration of whey, J. Membr. Sci. 332 (2009) 69–80.
[32] A.D. Marshall, P.A. Munro, G. Tragardh, Effect of protein fouling in microfiltration and ultrafiltration on permeate flux, protein retention and selectivity: a literature review, Desalination 91 (1993) 65–108.
[33] E. Matthiasson, Role of macromolecular adsorption in fouling of ultrafiltration membranes, J. Membr. Sci. 16 (1982) 23–36.
[34] M. Turker, J. Hubble, Membrane fouling in a constant-flux ultrafiltration cell, J. Membr. Sci. 34 (1987) 269–281.
[35] K.H. Keller, E.R. Canales, S.I. Yum, Tracer and mutual diffusion coefficients of proteins, J. Phys. Chem. 75 (1971) 379–387.